The Journal of
Undergraduate Research
in Physics

Volume 2, Number 1

April, 1983

Published by Guilford College
for
The American Institute of Physics and The Society of Physics Students

THE JOURNAL OF UNDERGRADUATE RESEARCH IN PHYSICS

This journal is devoted to research work done by undergraduate students in physics and its related fields. It is to be a vehicle for the exchange of ideas and information by undergraduate students. Information for students wishing to submit manuscripts for possible inclusion in the Journal follows.

ELIGIBILITY

The author must have performed all work reported in the paper as an undergraduate. The subject matter of the paper is open to any area of pure or applied physics or physics related field.

SPONSORSHIP

Each paper must be sponsored by a full-time faculty member of the department in which the research was done. A letter from the sponsor to the editor must accompany the manuscript if it is to be considered for publication.

FORM

The manuscript should be typed, double spaced, on 8 1/2 x 11 inch sheets. Margins of about 1 1/2 inch should be left on the top, sides, and bottom of each page. Papers should be limited to twelve pages of text in addition to an abstract and appropriate drawings, pictures, and tables.

GENERAL STYLE

All papers must conform to the Style Manual of the American Institute of Physics. Each paper must be prefaced by an abstract that does not exceed 250 words.

ILLUSTRATIONS

Line drawings should be made with black India ink on plain white paper. If a graph is drawn on co-ordinate paper, the paper must be lined blue. Important lines should be ruled in black. Each figure or table must be on a separate sheet. Photographs must have a high gloss finish.

CAPTIONS

A brief caption should be provided for each illustration or table, but it should not be part of the figure. They should be listed together at the end of the manuscript.

EQUATIONS

Equations should appear on separate lines and may be written in black India ink.

FOOTNOTES

Footnotes should be typed double spaced and grouped together in sequence at the end of the manuscript.

SUBMISSION

Two copies of the manuscript should be sent to:

Dr. Rexford E. Adelberger, Editor
THE JOURNAL OF UNDERGRADUATE RESEARCH IN PHYSICS
Physics Department
Guilford College
Greensboro, NC 27410

SUBSCRIPTION INFORMATION

The Journal will be published biannually with issues appearing in April and October of each year. There will be two issues per volume.

TYPE OF SUBSCRIBER	PRICE PER VOLUME
Individual	$ 5.00
Institution	$10.00

Foreign subscribers add $2.00 for postage

To receive a subscription, send your name, address, and check made out to The Journal of Undergraduate Research in Physics to:

Journal of Undergraduate Research in Physics
Physics Department
Guilford College
Greensboro, NC 27410

BACK ISSUES

Back issues may be purchased by sending $10.00 per volume to the editorial office.

ISSN 0731 - 3764

The Journal of Undergraduate Research in Physics is published by Guilford College for the American Insititute of Physics and the Society of Physics Students.

VOLUME 2 1983

The Journal of Undergraduate Research in Physics

Published by Guilford College
for
The American Institute of Physics and The Society of Physics Students

ISSN 0731 - 3764

THREE-DIMENSIONAL COMPUTER GRAPHICS USING SIMPLE VECTOR CALCULATIONS

Michael L. McMullen
Physics Department
University of North Carolina - Asheville
Asheville, NC 28804

ABSTRACT

The usual method for implementing three-dimensional graphics uses translations through matrix manipulations. After the data points have been rotated, they then must be mapped from three-space to two-space via a perspective transformation. This method is slow, requiring many trivial calculations, and does not transfer easily into assembly language for real-time interaction with a user. By forming a viewing point, a sight point, and a projection plane and determining where vectors locating the data strike the projection plane, one can achieve rotation and perspective in one calculation. This method requires the use of the basic mathematical and square root functions only once per frame. This allows for easy translation into machine language. The concepts behind this method and a working program written in PASCAL are presented.

BACKGROUND

In a recent research project involving pair conversion processes in strong magnetic fields (1), it became necessary to graphically depict contour integral representations of generalized Laguerre polynomials. These polynomials (2) are components of the attenuation coefficients for the conversion of photons to electron-positron pairs. What is special about the Laguerre polynomials is the difficulty in representing them asymptotically.

A generating function (2) can be used to derive the various contour integral representations of the Laguerre polynomials.

$$W(\zeta,t)=\frac{1}{(1-t)^{\alpha+1}}e^{\frac{-\zeta t}{1-t}}=\sum_{n=0}^{\infty}L_n^{\alpha}(\zeta)t^n$$

It is possible to regard this series as an expansion about the origin in the complex t plane. Using a Laurent expansion and Cauchy's integral theorem, the polynomials may be expressed as contour integrals in the following fashion:

$$L_n^{\alpha}(\zeta)=\frac{1}{2\pi i}\oint dt\,\frac{1}{(1-t)^{\alpha+1}}e^{\frac{-\zeta t}{1-t}}\frac{1}{t^{n+1}}$$

The saddle point method is then used to find approximations to the contour integral and hence the Laguerre polynomials. This is the point at which three-dimensional graphics were found to be useful. The saddle point method requires a function that rises sharply about one point and remains stable throughout the rest of the domain. The steepest part of the ascent is used in calculating the approximation. The graphic representation is used as a visual aid to find the steepest path to allow for a more accurate approximation.

Creating three-dimensional representations of the Laguerre polynomials was a difficult task, not only due to the long computational time required to generate the display, but also because many different view points had to be presented to find the best path for the contour integrals. Using the existing method of matrix manipulations to translate and rotate the plot in each axis followed by a scaling and translation would have required, in the worst case, five matrix manipulations per data point in a graph consisting of over 1500 points. This does not include the steps needed to calculate angles of rotation nor the perspective transformation needed for each point. Clearly, a solution to the graphics problem that required fewer calculations had to be found if the Laguerre polynomials were to be done on a small computer.

OVERVIEW

An easier solution did exist and only required viewing the problem in a different light. Instead of using a fixed viewing coordinate system and rotating the object to find the points of interest, it was possible to form a flexible viewing system that could be moved around the stationary object. The process is outlined below.

A point in space (see Figure 1) is picked to be the sight point (S). Another point in space (O) is picked as the origin of the projection plane. The unit vector $\hat{A}$ from the origin point of the projection plane to the sight point is calculated. This vector will be normal to the surface of the projection plane. The viewing point (V) is a known distance (|V|) from the origin point in the direction opposite to $\hat{A}$. The projection plane is determined by finding a pair of orthogonal unit vectors ($\hat{PX}$ and $\hat{PY}$) that are perpendicular to $\hat{A}$. The components of the vectors from the viewing point to the data points are then calculated. The points where these vectors intersect the projection plane are the points that make up the two-dimensional representation of the three-dimensional object.

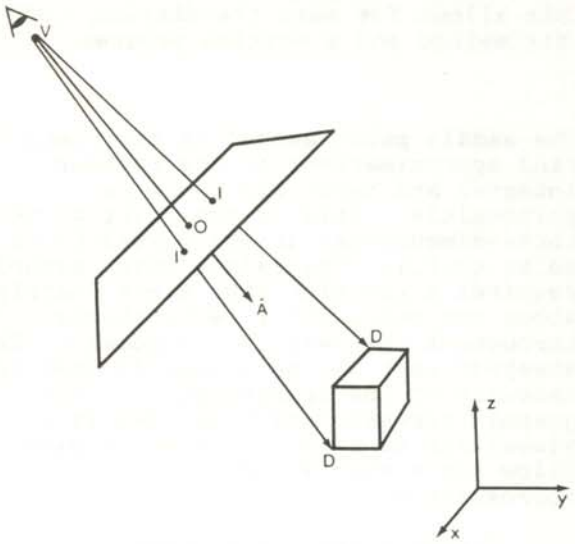

Figure 1
Layout of system showing the view point V, the line of sight unit vector $\hat{A}$, the projection plane and the object.

THE PROJECTION PLANE AXES

The creation of the coordinate axes for the projection plane is the most difficult aspect of the process. Fortunately, it needs to be done only once per picture. It is essential that the axes point in the proper directions no matter how the sight and viewing points are chosen. For example, if the sight point is located at (0,0,0) and the viewing point is located at (1,0,0), the projection plane's X axis ($\hat{PX}$) should point in the positive Y direction. If, on the other hand, the sight and viewing points were interchanged, $\hat{PX}$ should point in the negative Y direction. The same situation occurs for the Y axis of the projection plane ($\hat{PY}$). This is shown in Figure 2.

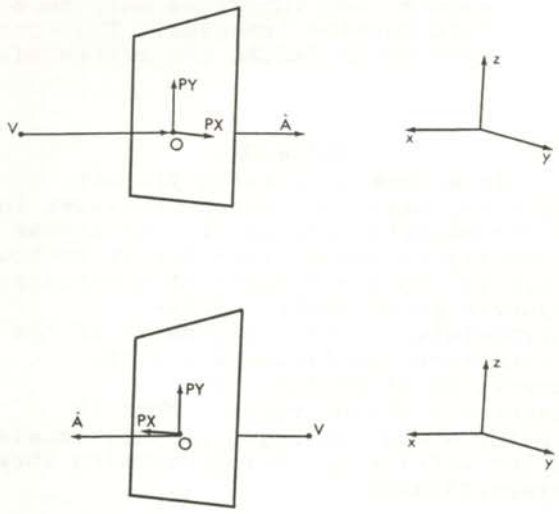

Figure 2
The unit vectors $\hat{PX}$ and $\hat{PY}$ defining the projection plane and their relationship with the line of sight unit vector $\hat{A}$ is shown.

The components of $\hat{PX}$ = (a,b,c) and $\hat{PY}$ = (d,e,f) can be calculated from the components of the unit vector A = (α , β, γ) using the following conditions.

a. The $\hat{PX}$ axis must lie in the XY plane of the chosen co-ordinate system. This means that

$$c = 0.$$

b. PX and PY have unit length or,

$$\hat{PX} \cdot \hat{PX} = 1, \quad \hat{PY} \cdot \hat{PY} = 1.$$

c. $\hat{PX}$ and $\hat{PY}$ are orthogonal vectors or,

$$\hat{PX} \cdot \hat{PY} = 0.$$

d. The projection plane points in the direction of sight $\bar{A}$ or,

$$\hat{PX} \times \hat{PY} = \hat{A}.$$

These vector relationships yield the following five equations for the five remaining unknown components of the projection plane axes vectors:

$$a^2 + b^2 = 1$$

$$ad + be = 0$$

$$-bf = \alpha$$

$$af = \beta$$

$$bd - ae = \gamma$$

Solving these equations for the components of the projection plane axes in terms of the known components of the viewing unit vector $\bar{A}$ yields:

$$a = \frac{\beta}{\sqrt{\alpha^2+\beta^2}}$$

$$b = \frac{-\alpha}{\sqrt{\alpha^2+\beta^2}}$$

$$c = 0$$

$$d = \frac{-\alpha\gamma\sqrt{\alpha^2+\beta^2}}{\alpha^2+\beta^2}$$

$$e = \frac{-\beta\gamma\sqrt{\alpha^2+\beta^2}}{\alpha^2+\beta^2}$$

$$f = \sqrt{\alpha^2+\beta^2}$$

These solutions are correct for any given sight point and viewing point except for the case where α and β are both equal to zero. This does not create any real limitations as either α or β may approach zero as closely as the accuracy of the computer allows.

DETERMINING THE VISIBLE POINTS

$\bar{B}$ is the vector (see Figure 3) between the viewing point and the data point. The vector $\bar{V}$ is the vector along the line of sight between the viewing point and the origin of the projection plane. If the distance (B') from the viewing point (V) to the intersection point (I) can be found, then that distance divided by $|\bar{B}|$ will give a parameter (Bt) that determines if the point is visible. Examination of Figure 3 shows that the distance B'

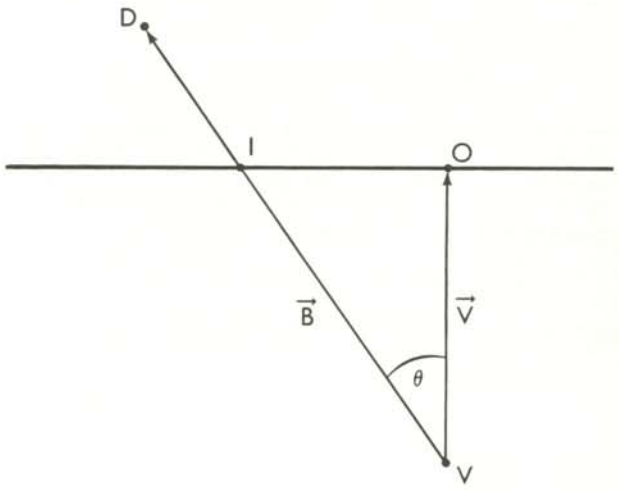

Figure 3
Relationship between the data point D, the vectors $\bar{B}$ and $\bar{V}$. The distance between V and I is B'.

is equal to the size of vector V divided by the cosine of the angle between V and B. This gives the following equation for B'

$$B' = \frac{|\bar{V}|^2 \, |\bar{B}|}{\bar{V} \cdot \bar{B}}$$

Dividing B' by $|\bar{B}|$ gives the parameter Bt.

$$Bt = \frac{|\bar{V}|^2}{\bar{V} \cdot \bar{B}}$$

It should be noted that $|\bar{V}|$ is a constant that is determined at the beginning by the user. Therefore, the only calculation required to be done is the dot product.

If Bt is greater than one, the point is between the projection plane and the view point and cannot be seen. If Bt is less than or equal to zero, then the view point is between the projection plane and the data point. This too means that the point is not visible. The data point will only be visible if Bt is between zero and one.

CALCULATION OF TWO-SPACE COORDINATES

The calculations up to this point have all taken place in three-space. What remains to be done is the transformation of these three-space points to two-space points. As seen in Figure 4, the vector $\bar{I}$ locates the point to be plotted with respect to the origin of the perspective plane. It is clear that

$$\bar{I} = \bar{B}' - \bar{V},$$

where $\bar{B}'$ is the vector from the view point to the intersection point I. The components of $\bar{B}'$ can be found in terms of the known components of $\bar{B}$ and the parameter Bt in the following way.

$$\bar{B}' = (B') \bar{B}/|\bar{B}| = (Bt)\bar{B}$$

so

$$\bar{I} = (Bt)\bar{B} - \bar{V}$$

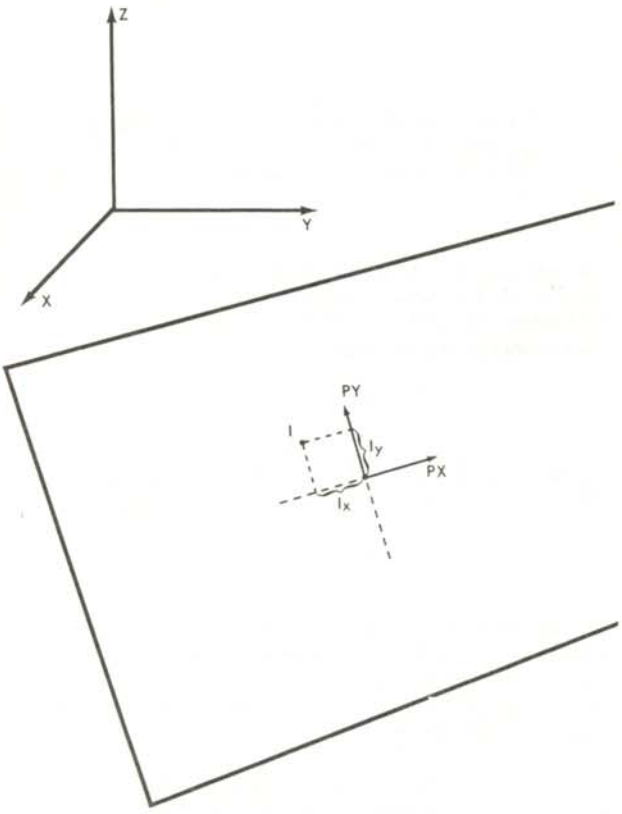

Figure 4
How the intersection point I determines the coordinates of the point to be plotted on the projection plane.

The points Ix and Iy to be plotted then can be found by taking the dot product of the vector $\bar{I}$ and the axes of the projection plane.

$$Ix = \bar{I} \cdot \hat{PX}$$

$$Iy = \bar{I} \cdot \hat{PY}$$

Figure 5 is an example of the graphics that can be generated using this method. The total calculating-plotting time for this picture was just under 30 seconds.

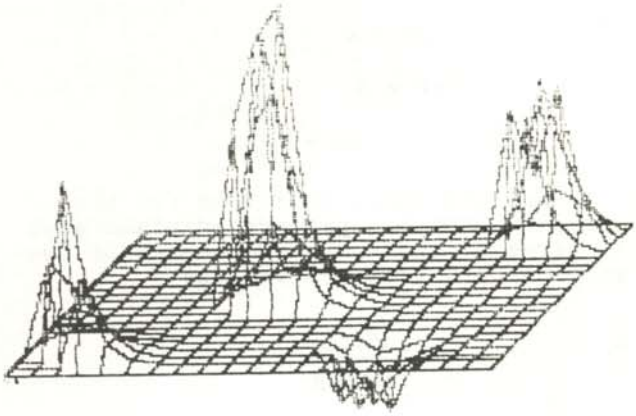

Figure 5
An example of a graphics output using this technique. The whole calculation took less than 30 seconds to complete.

CONCLUSION

A mathematically simple and quick algorithm for producing a two-dimensional image with perspective of a three-dimensional object has been derived. Because the procedure does not require matrix manipulations, it easily can be coded into machine language. This process is currently being translated into Z-80 assembly language to allow real-time applications.

Listing 1 is a program written in PASCAL that will open a file that contains data points in three dimensions that define some object. The user specifies the view and sight points. The routine then generates the graphic display at that perspective. This routine can be translated into any other high level computer language.

Listing 1
This is a listing of a PASCAL program that will convert a file containing the location in three dimensions of an object to a two-dimensional display from a perspective chosen by the user.

```
PROGRAM PROJECT(INPUT,OUTPUT);

USES
     TRANSCEND, TURTLEGRAPHICS;

CONST
     VIEWDIST=1600.0;

TYPE
     POINTDATA=RECORD
                 X,Y,Z:REAL;
                 PEN:BOOLEAN
               END;

VAR
     SIGHTX,SIGHTY,SIGHTZ:REAL;
     VIEWX,VIEWY,VIEWZ:REAL;
     AX,AY,AZ:REAL;
     TVD,BTPARM:REAL;
     ORIGINX,ORIGINY,ORIGINZ:REAL;
     DATAX,DATAY,DATAZ:REAL;
     BX,BY,BZ:REAL;
     DOTPROD:REAL;
     INTERX,INTERY,INTERZ:REAL;
     A,B,XX,XY,XZ,YX,YY,YZ,:REAL;
     PX,PY,PZ,XCORD,YCORD:REAL;
     UAX,UAY,UAZ:REAL;

     X1,Y1:INTEGER;

     DATA:POINTDATA;

     DATAFILE:FILE OF POINTDATA;

FUNCTION DOT(A,B,C,D,E,F:REAL):REAL;

     BEGIN
        DOT:=A*B+C*D+E*F
     END;



PROCEDURE SETUP;

     BEGIN
        WRITE('SIGHT POINT=');
        READLN(SIGHTX,SIGHTY,SIGHTZ);

        WRITE('VIEWPOINT=');
        READLN(ORIGINX,ORIGINY,ORIGINZ);

        (* FORM VECTOR FROM ORIGIN POINT TO
        SIGHT POINT *)

        AX:=SIGHTX-ORIGINX;
        AY:=SIGHTY-ORIGINY;
        AZ:=SIGHTZ-ORIGINZ;

        (* FIND THE DISTANCE FROM THE ORIGIN
        POINT TO THE SIGHT POINT *)

        TVD:=SQRT(AX*AX+AY*AY+AZ*AZ);

        (* FIND THE UNIT VECTOR A *)

        UAX:=AX/TVD;
        UAY:=AY/TVD;
        UAZ:=AZ/TVD;

        (* CALCULATE VIEW POINT OF PROJECTION
        PLANE *)

        VIEWX:=ORIGINX-UAX*VIEWDIST;
        VIEWY:=ORIGINY-UAY*VIEWDIST;
        VIEWZ:=ORIGINZ-UAZ*VIEWDIST;

        (* CREATE VECTOR FROM VIEW POINT *)

        AX:=ORIGINX-VIEWX;
        AY:=ORIGINY-VIEWY;
        AZ:=ORIGINZ-VIEWZ;

        (* MUST FORM X-Y COORDINATE SYSTEM.
        THE THREE-SPACE POINT STRIKES THE
        PROJECTION PLANE.
        X VECTOR WILL BE X AXIS,
        Y VECTOR WILL BE Y AXIS *)

        A:=UAX*UAX+UAY*UAY;
        B:=SQRT(A);

        XX:=UAY/B;
        XY:=-UAX/B;
        XZ:=0

        YX:=-UAX*UAZ*B/A;
        YY:=-UAZ*UAY*B/A;
        YZ:=B;

     END;



PROCEDURE CONVRT2D;

     BEGIN

        (* GET DATA POINT *)

        DATAX:=DATA.X;
        DATAY:=DATA.Y;
        DATAZ:=DATA.Z;

        (* FORM VECTOR FROM VIEWING
        POINT TO DATA POINT *)

        BX:=DATAX-VIEWX;
        BY:=DATAY-VIEWY;
        BZ:=DATAZ-VIEWZ;

        (* CALCULATE DOT PRODUCT *)

        DOTPROD:=DOT(AX,BX,AY,BY,AZ,BZ);

        BTPARM:=VIEWDIST*VIEWDIST/DOTPROD;

        (* PLUG BTPARM INTO EQUATION FOR LINE
        BETWEEN VIEWING POINT AND DATA POINT
        AND FIND COORDINATES WHERE LINE
        INTERSECTS THE PLANE. *)

        INTERX:=VIEWX+BX*BTPARM;
        INTERY:=VIEWY+BY*BTPARM;
        INTERZ:=VIEWZ+BX*BTPARM;

        (* FORM POINT VECTOR *)

        PX:=INTERX-ORIGINX;
        PY:=INTERY-ORIGINY;
        PZ:=INTERZ-ORIGINZ;

        (* CALCULATE X-Y COMPONENTS *)

        XCORD:=DOT(PX,XX,PY,XY,PZ,XZ);
        YCORD:=DOT(PX,YX,PY,YY,PZ,YZ);

     END;
```

```
PROCEDURE GRAPH;

     BEGIN;

        X1:=TRUNC(XCORD)+140;
        Y1:=TRUNC(YCORD)+96;

        IF DATA.PEN
                THEN PENCOLOR(WHITE)
                        ELSE PENCOLOR(NONE);

        MOVETO (X1,Y1)

     END;



   PROCEDURE CALCPNT;
        BEGIN

           (* CALCULATE DATA POINTS *)

           WHILE NOT EOF(DATAFILE) DO
                   BEGIN
                           DATA:=DATAFILE^;
                           GET(DATAFILE);
                           CONVRT2D;
                           GRAPH
                   END

        END;

   BEGIN (* MAIN DRIVER *)

        SETUP;
        RESET(DATAFILE,'DATA1:KLEPIKOV.DATA');

        INITTURTLE;
        PENCOLOR(NONE);

        CALCPNT;
        CLOSE(DATAFILE);
        READLN;
        TEXTMODE

   END.
```

ACKNOWLEDGMENTS

The author would like to acknowledge the support and advice provided by Dr. Joseph K. Daugherty.

REFERENCES

(1) Daugherty, J.K. and Harding, A.K., Astrophysical Journal, in press (1983).

(2) Abramowitz, M. and Stegun, I., Handbook of Mathematical Functions, Dover Publications, (1965).

FACULTY SPONSOR FOR THIS PAPER

Dr. J. K. Daugherty
Physics Department
University of North Carolina - Asheville
Asheville, NC 28804

THE USE OF HIGH-VOLTAGE PHOTOGRAPHY AS A TECHNIQUE FOR DETECTING SUB-SURFACE ELECTRICAL INHOMOGENEITIES IN MATERIALS*

Rodney Rountree
Physics Department
University of North Carolina at Wilmington
Wilmington, NC 28405

ABSTRACT

This paper investigates the ability of high-voltage photography (HVP) to detect sub-surface electrical inhomogeneities independent of the surface smoothness. A method is devised in which samples could be tested with controlled deviations in surface smoothness. This method was used to examine the ability of HVP to resolve differences in the conductivity of materials which have no surface correlations. The findings of this study indicated that it was possible to detect sub-surface electrical inhomogeneities and that changes in resistivity can also be detected. Finally, a theory is discussed which offers an explanation for the observed dependence of the discharge on frequency, the occurence of unexpected areas of no discharge, and explains why HVP can be used to detect variations in resistivity.

INTRODUCTION

High-voltage photography (HVP) is known by several names: Corona Discharge Photography; Electrical Discharge Imaging; and most commonly, Kirlian Photography. The technique first gained fame as the result of the work of Seymon Kirlian who began his studies of the technique in Russia during the 1930's (1). His work was with living subjects and resulted in the Russian idea of a bioplasm (2). In the United States Dr. Thelma Moss, of the University of California at Los Angles, was greatly influenced by the Russian's work. Her research brought much attention to the technique with which she claimed to detect an unknown life force (3). In the process of trying to understand the technique and put it on a more scientific footing, physical, rather than living samples were examined. This led to important advances in the 1979's in understanding the HVP technique and its use in materials testing.

HVP is a process in which a photograph of an object is taken in complete darkness. The light needed to expose the film is produced by an induced corona discharge. A type of device for making these pictures is shown in Figure 1. With this device, the object to be photographed is placed in direct contact with the film. Under the film is an insulation plate, usually glass, that helps protect the film from being overexposed. Under the insulation plate is an electrical conductor, such as a copper plate, which is connected to a negative high-voltage source.

The method of corona discharge formation has been studied thoroughly and is a well known phenomenon (4). The applied high voltage causes electrons to jump into the air gap

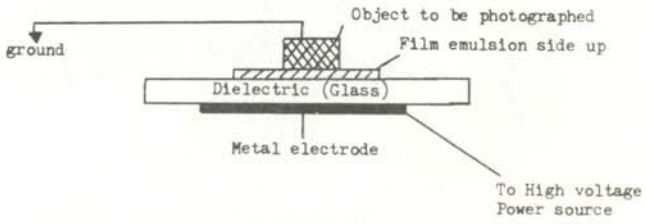

Figure 1
A simple device for making HVP pictures.

between the the cathode and the object (which serves as the anode). When these electrons acquire enough energy, they begin to travel across the air gap towards the anode, ionizing the surrounding air and producing an avalanche effect along the way. The density of the positive ions left behind soon becomes sufficient to pull some of the electrons back from the

anode and recombination events occur. These cause the emission of light which exposes the film. Electrical breakdown occurs across the gap as a result of the propagation of additional avalanches by the secondary process (5).

In their study of HVP, Boyers and Tiller (6) showed that the pattern of the positive-negative streamer formation is strongly dependent on the time the high voltage is applied (pulse width), the number of pulses, and the inter-electrode spacing. It is only weakly dependent on the type of electrode material used. Here perhaps the most important (and often subtle) parameter is the inter-electrode spacing. This spacing is defined as the distance from the cathode to the anode. This distance has a large variation over the surface area due to deviations from absolute smoothness (7). This effect is evident in the great detail of the surface relief evident in the photographs of the two coins shown in Figure 2.

Lord (8) goes a step further in his studies and describes the use of HVP as a technique for materials testing. He proposes that the technique can be used to reveal or amplify surface and sub-surface conditions of the materials being tested. He also suggests that it

Figure 2
Negative pictures of coins taken using HVP. These are exposed directly onto photographic paper. The darker areas are the regions where most light is produced. The pale area of the face results from direct contact with the emulsion surface.

is sensitive to impurities and porosities in the material. In one of the experiments described by Lord and Petrini, a nickel specimen with hardness indents is photographed from both sides. The photograph of the indented side showed the indents as light areas surrounded by dark circles. The other side, with no visible indication of indents, revealed the indents as black spots surrounded by gray areas (9). Nielson and Schackelford suggested that this indicated deviations from surface smoothness as opposed to evidence of sub-surface stresses (10).

An extremely interesting experiment performed by Lord and Petrini (11) was not so easily explained. An aluminum bar with milling marks was polished smooth until no evidence of the marks were detectable either by visual or mechanical inspection. HVP pictures of the bar revealed the milling marks. Lord attributed this to the technique's ability to detect the sub-surface internal state of the metal (12).

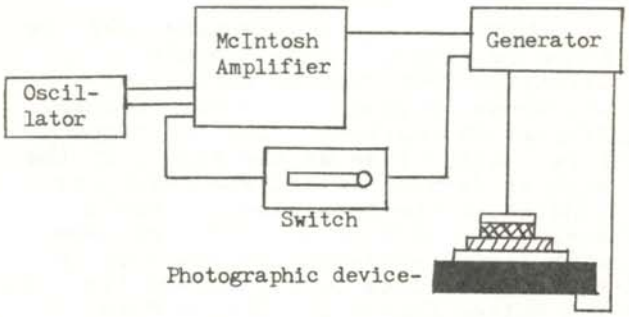

Figure 3
Equipment used to make HVP pictures.

It is apparent that there is a disagreement. Lord and Petrini claim that HVP can be used to detect sub-surface characteristics of materials (13), while Nielsen and Schakelford hold that the patterns in HVP are caused by micro-deviations in surface smoothness (14). The primary goal of this research is to determine if HVP can be used to detect sub-surface characteristics of materials independently from their surface characteristics. A second goal is to determine if differences in the electrical impedance of materials can be detected using HVP.

MATERIALS AND METHODS

A diagram of the equipment used in this study is shown in Figure 3. The amplifier is used to set the applied

voltage. The applied voltage could be held relatively constant by observing the length of the streamers through the spark gap, but it was difficult to measure with any accuracy. The frequency of the output voltage was controlled by the oscillator and the pulse width by a tap switch. The power source was connected to the photographic device shown in Figure 1. The electrical breakdown occurs in the air gap between the object to be photographed and the copper plate. With this apparatus, photographs were taken of various materials under different conditions. Exposures were made on 4 in. x 5 in. Kodak Tri-X pan sheet film or directly onto photographic paper.

A number of different techniques for constructing samples were investigated in the process of finding a way to keep the surface conditions constant. The first attempt consisted of a pencil drawing of a fish. Another attempt was to photograph a poly-crystalline silicon plate with boron doped crystal interfaces. It was hoped that the slightly higher electric field produced at the crystal interfaces could be detected. Due to the small size and complexity of the silicon sample, it was decided to experiment with samples that had more obvious electrical gradients.

In the second set of sample constructions, objects of differing electrical characteristics were sandwiched between two sheets of opaque graphite paper and then sealed with photographic sealing tape. Four different samples were made. In the first, a hole was cut in a piece of graphite paper and filled with a piece of plain non-conducting paper. This sample was sandwiched as indicated above. In the second attempt, an aluminum triangle with a height of 2.5 cm was placed in the graphite paper sandwich. The next sample contained several 1 cm triangles. This was used to determine the resolution of the apparatus. The final of this style construction was an aluminum foil on which liquid graphite was painted. A second aluminum square was placed over the painted one, and this was sandwiched in the usual way. There was a common problem with all these techniques, i.e. none of them controlled the surface deformation caused by the sandwiched material or kept the inter-electrode spacing constant.

The solution to this problem was to use a cleaved piece of mica to control the surface smoothness. On this substrate, metal deposits were made (Figure 4). First, copper was deposited to a desired thickness. A

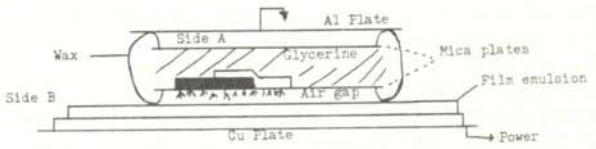

Figure 4
Sample construction used when making photographs under conditions with controlled surface relief.

second material was then deposited to test the effects of varying thicknesses and conductivities. A second mica plate and glycerine were used as a protective covering. This improved sandwich was then sealed with wax. The wax formed an air gap in which the discharge could take place. With this set-up, photographs could be taken from side A to illustrate differences in inter-electrode spacing and surface relief. A photograph taken from side B had these parameters constant. This type of sample preparation was used to examine the ability of HVP to resolve differences in the conductivity of materials that had no surface correlations.

With the improved construction, a series of photographs were taken of two 5×10^{-8} m. thick films of copper and bismuth. The mica substrate was covered by four alternating layers of copper and bismuth. The side A pictures had a maximum inter-electrode spacing and surface relief of 1.5×10^{-7} m. while those of side B had a constant surface relief.

Since the reflectivity of the material is a factor in the image produced, a better method for analyzing the photograph was devised. The number of streamers per square centimeter for each area of the picture was counted (see Figure 5). The averages were determined for 6 runs in the frequency range 500 - 1400 Hz. and 5 runs in the frequency range 1000 - 1800 Hz.

RESULTS

Figure 6 shows the pencil drawing of a fish on paper. The most striking feature is the lower part of the tail. It had been erased and then redrawn. The erased area shows up clearly. The photograph shown in Figure 7c of the silicon plate shown no crystalline interfaces. When the frequency at which the picture is made is reduced from 1000 Hz to 10 Hz, there is a dramatically different discharge pattern (see figure 7a). This photograph shows clearly the depression of the silicon plate in the center due to the heavy ground connection on the top. This deformation of the plate causes a smaller air gap in the center. This results in a low density of streamers and the indistinct shadows typical of glow discharge. The density

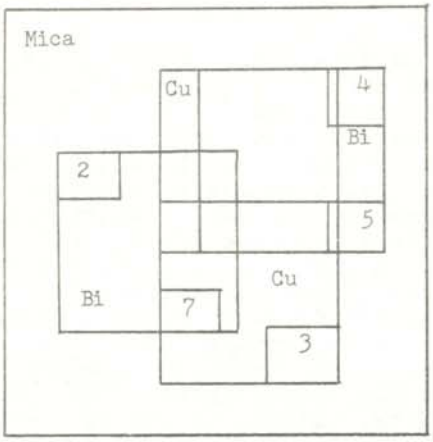

Figure 5
Areas used to quantify the amount of discharge caused by a material.

of streamers and glow discharge is seen to increase in the picture taken at 100 Hz (Figure 7b), but the image of the depression is lost. Figure 8 is a picture taken of the plate after it was cracked. The crack can be seen extending across the middle of the picture.

Figures 9, 10, and 11 are of the graphite sandwich samples. The cut out sample is clearly seen in Figure 9. The area of the hole can be seen in the center of the picture as an area of high discharge surrounded by an area of poor discharge. The 2.5 cm aluminum triangle is seen in Figure 10a as an area of no discharge surrounded by areas of discharge. The 1 cm triangles are barely visible in the center of Figure 10b. The sample of aluminum foil sandwiching the liquid graphite is shown in Figure 11. The aluminum area is clearly seen as being without discharge, while the area painted with graphite appears exactly like that of the surrounding paper.

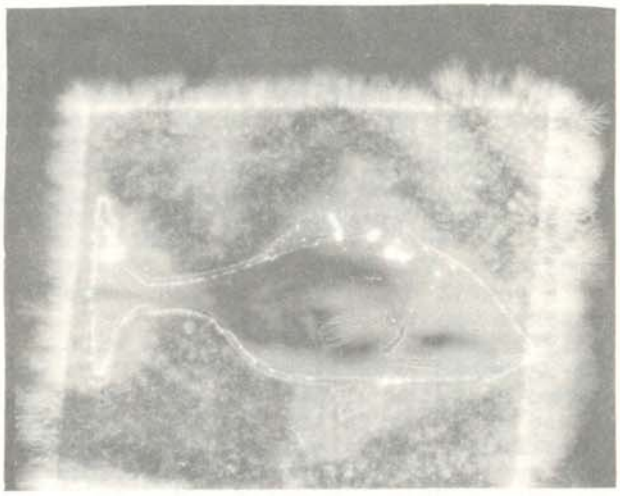

Figure 6
HVP picture of a pencil drawing of a fish on paper. Note the lower portion of the tail which had been erased and redrawn.

Photographs of samples made using the final construction technique are shown in Figures 12 and 13. Figure 12 shows the samples taken from side A. Ignoring the first copper deposit, no distinct border is seen that would indicate a change in thickness or type of material. Photographs of the same sample taken from side B (in which surface relief is controlled) are seen in Figure 13. The area of the second bismuth layer has a different pattern than the others. The picture is dominated by larger, more diffuse, streamers. A graph of the average streamer density for an area over the entire frequency range in which the the discharge occurred versus resistivity is shown in Figure 14.

There was a correlation between the voltage at which the pictures were made and the frequency range over which there was discharge. The voltage did

not cause any other differences that were detectable with this apparatus. The frequency, however, had a major effect on the amount of discharge produced for a given sample. This is shown well in Figures 7, 12, and 13. It was observed that different impedance materials produce discharges over different frequency ranges. Another general characteristic is that

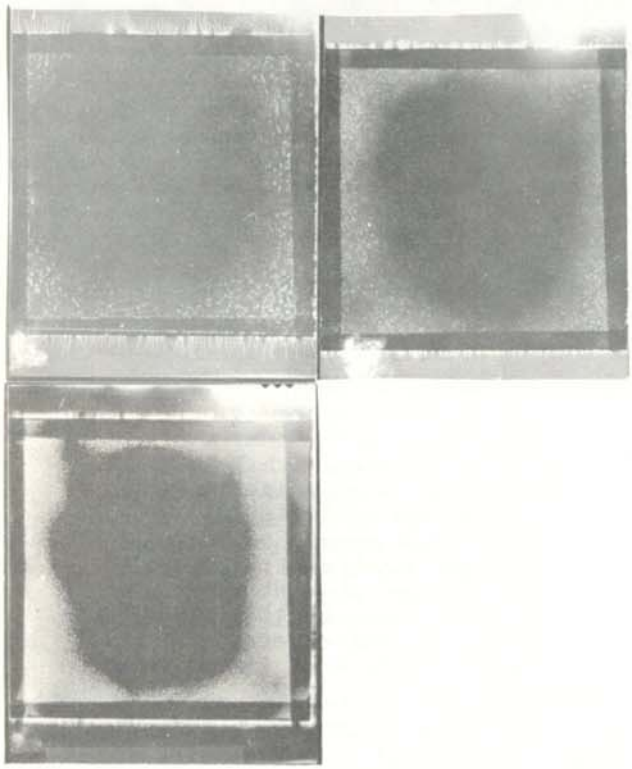

Figure 7
HVP pictures of a polycrystalline silicon plate with boron doped interfaces. The deformation of the plate can been seen in part a. Note the changes in the streamer formation with frequency.

a large portion of the photographs have areas that lack any form of discharge (for example, see Figure 7).

DISCUSSION OF RESULTS

To show how some of the parameters affect the pattern of corona discharge, a picture of a leaf is shown in Figure 15. The surface relief is greatest along the veins of the leaf. The ridges there increase the local electric field. This decreases the sparking potential, creating more discharge along the vein. An increase in the air gap causes a decrease in the discharge. However, the increase in the air gap causes an increase in the density of the streamers in a clustering manner because there is more time for branches to form off the main streamer.

The erased area of the fish drawing (Figure 6) is easily visible. This could be caused by the presence of some un-erased graphite giving the area a lower conductance or by a ridge formed by the pencil trace. Either of these effects would cause the pattern seen.

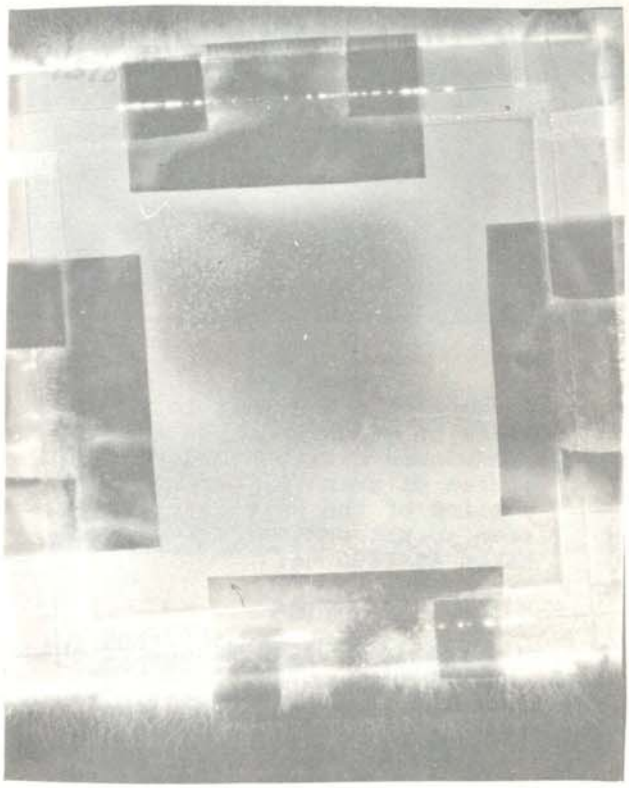

Figure 8
Photographs of the silicon plate after it was cracked. The crack can be seen extending through the middle of the picture (taken at 1000 Hz).

The pictures of the silicon plates show no edges. This is probably caused by the relatively large resolution of the technique. An interesting effect that can be seen in these pictures is the dependence of the discharge pattern

on the frequency of the applied voltage and the presence of a depression pattern (Figure 7). The dependence of the discharge on frequency was noted by Nielsen (15) and will be discussed later. The ability of the HVP technique to detect the depression in the silicon plate is interesting, but the manner in which the pattern is formed is even more fascinating. As seen in Figure 7a, the pattern is

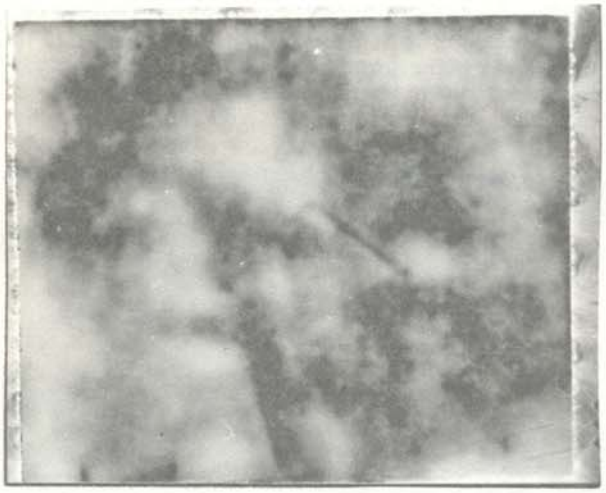

Figure 9
Picture of a hole cut in a piece of graphite paper and sandwiched between two other pieces of graphite paper. The outline of the hole is clearly seen in the center picture taken at 1000 Hz.

composed mainly of glow discharge and a small amount of streamer discharge. The discharge is confined within regions resembling an interference pattern. One would expect a gradual change in the density of the pattern. The discrete areas of discharge are unexplained, but may involve the effects of an actual interference in the local concentration of photo-ionization.

The photographs of the hole out of a piece of graphite paper show the surface geometry. A ridge would develop at the edge of the cut forming the outline of the hole. The photographs of the aluminum triangles do not give the expected results. Because the bulge in the surface relief tends to be rounded, one would expect an indistinct border between the aluminum and graphite areas. What one sees, however, is that the aluminum area completely lacks discharge. The small aluminum triangles (Figure 10b) show well the limit of resolution of this HVP apparatus. They are barely visible. It is therefore clear why the crystal interfaces in the polycrystalline plates did not show up in the pictures.

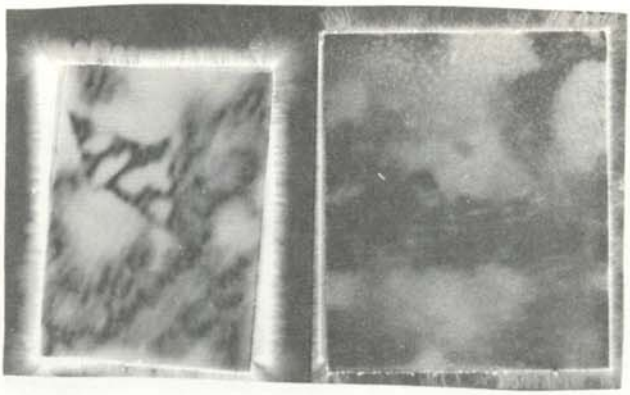

Figure 10
Photographs of aluminum triangles sandwiched between two sheets of graphite paper. The large triangle in the upper left hand corner of picture a and the smaller triangles in the center of picture b are clearly seen at 1000 Hz. The small triangles show the limit of resolution of the apparatus.

The most interesting photographs from the graphite paper series were those that had the sandwiched Aquadag (liquid graphite) and aluminum foil (Figure 11). The aluminum area is clearly seen to be without discharge, while the center area of the Aquadag appears the same as that of the surrounding graphite paper. If the picture were caused by surface effects, one would expect a gradual transition from the pattern of the graphite to that of Aquadag. The aluminum area should appear intermediate to the other two areas.

Instead, the areas of graphite paper appear to have a pattern independent of the thickness, while the aluminum area is dramatically different. It should be noted that the Aquadag is seen through the aluminum. This is strong evidence of HVP's ability to distinguish between the electrical characteristics of materials independently from the surface geometry.

These results show the need to have samples that have controlled surfaces so that one can check if indeed HVP can detect subsurface effects. The construction technique that uses the cleaved mica plates as a substrate meets this need. The

Figure 11
Photograph of Aquadag painted between two squares of aluminum foil and sandwich between two sheets of graphite paper. In all cases, the areas of graphite produce the same discharge pattern.

deposition of samples on the rigid mica plate controls the surface relief. It also controls the inter-electrode spacing and air gap due to the rigidness of the plate. One must be careful that the top plate is set parallel to the bottom one. If not, the thickness of the air gap will vary from one side to the other causing a change in the pattern.

Figure 12 shows that HVP can be used to detect copper and bismuth deposits through the mica plates. Because the surface conditions are controlled, this indicates that subsurface characteristics can be detected. Since there is no air gap between the deposits and the mica plate, streamers in the area of the sample must be generated from the surface of the mica. The conclusion that the pattern is not caused by any changes in the surface relief is supported by the similar discharge pattern for the area in pictures taken from side A (Figure 13) where the surface relief has a maximum variance of 1.5×10^{-7} m.

In the course of this study, it was noticed that for a given sample, discharge would occur only over a specific frequency range when the voltage was held constant. As the frequency increased, the discharge would increase. When some peak

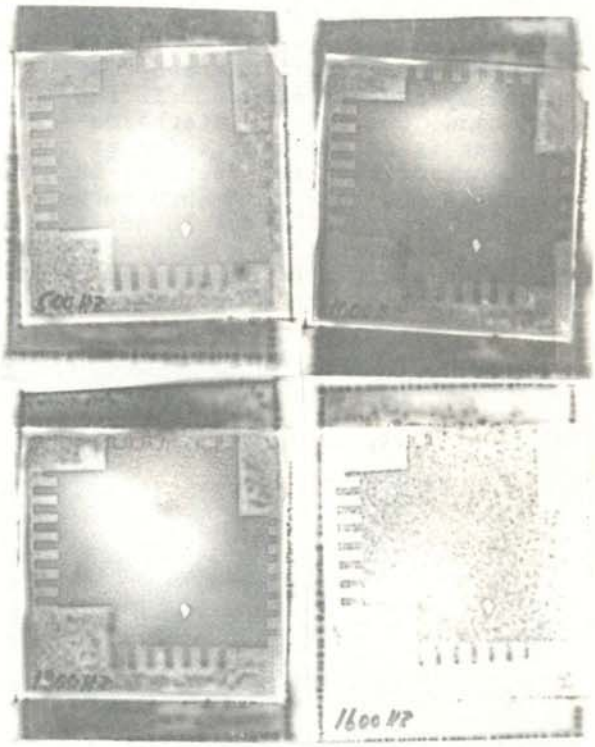

Figure 12
Negative prints of copper-bismuth deposits on mica. These are taken from side A so that the surface relief is not controlled. Clockwise from the upper left hand corner, the frequency applied is as follows: 500 Hz, 1000 Hz, 1300 Hz, and 1600 Hz.

frequency was reached, any increase in frequency caused a decrease in the amount of discharge. Varying the voltage only had the effect of shifting the peak frequency. When the voltage reached a certain level, an apparent saturation level was reached and the peak in the discharge-frequency spectrum no longer shifted to higher values.

A reason for this frequency dependence was suggested when it was discovered that the frequency range over which the discharge occurred could be dramatically increased by adding a large resistance to the sample. It became clear that as the impedance of the output transformer changed with frequency and load, the current passing through the sample changed too. As the frequency increased, the load on the transformer increased, and the current passing through the air gap increased. This caused the rise in the discharge - frequency spectrum. The drop was caused by another effect. If the quenching time for the discharge streamer is on the same order as the frequency of the high voltage, then the stream is not able to quench between pulses. If the streamer is not able to quench, recombination events would be inhibited and hence there would be no light to expose the film. Therefore, one should see an increase in discharge with frequency due to the increase in the current. At some point, the quenching time becomes longer than the pulse length, and the discharge decreases because no recombination occurs. Thus the peak in the discharge-frequency spectrum is explained.

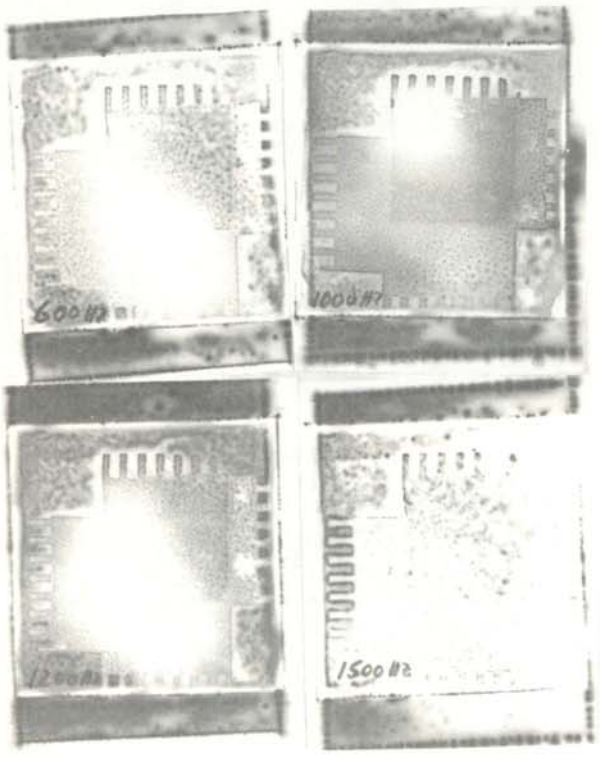

Figure 13
Negative prints of copper-bismuth deposits on mica taken from side B so that the surface relief is controlled. The frequency at which the pictures were taken is: a - 600 Hz, b - 1000 Hz, c - 1300 Hz, and d - 1500 Hz.

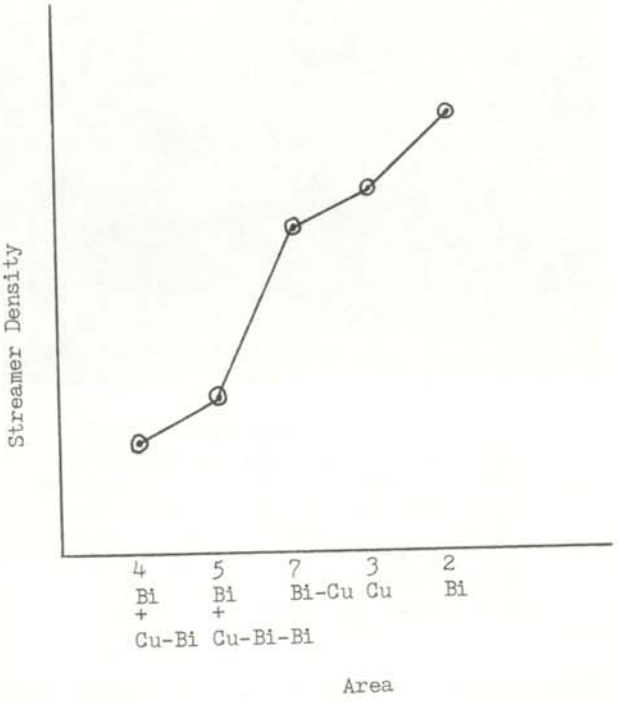

Figure 14
Graph of material type vs. streamer density. The materials are shown in order from the mica surface. For example, area 7 is composed of a copper layer over a bismuth layer on the mica. Hence the bismuth layer has the greatest effect on the discharge. The differences between areas 4 & 5 and 2 & 3 is caused by a tilt in the mica plate. It appears that areas with more bismuth have higher discharge densities.

The same reasoning may also be used to explain the patches of no discharge which occur in nearly all of the photographs taken. Boyers and Tiller (16) suggested that this pattern

was caused by buckling of the film. This is unlikely in our pictures that use the mica substrate. There is a strong correlation between the location of these blank areas and the location of the ground contact to the aluminum ground plate. If this is the case, then the contact is being detected through the air gap, two mica plates, the sample and an aluminum plate - a distance of more than 1 mm. This area produces a strong electric field and current flow from the contact. In this region, the charge density remains high and does not allow quenching, even at low frequencies.

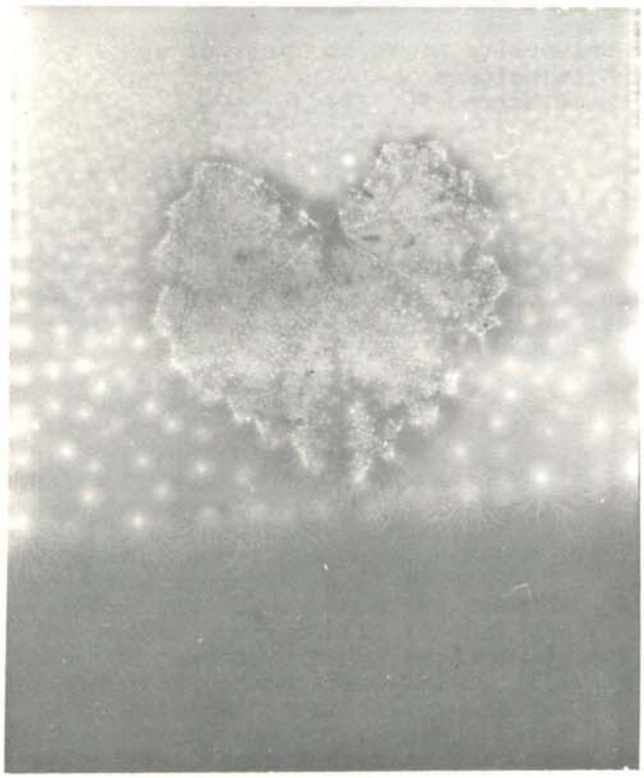

Figure 15
HVP photograph of a leaf, illustrating how several parameters affect the discharge pattern.

CONCLUSIONS

The findings of this study support the work of Lord and Petrini. It was possible to detect subsurface electrical inhomogeneities in materials that have no correlation with the surface characteristics. It was found that areas of differing electrical characteristics produce different discharge patterns. Preliminary data from this study also suggest that materials of different resistivities can be detected. There is a direct dependence between the average streamer density over the entire frequency range and the resistivity of the material.

Finally, a mechanism is suggested for explaining the observed discharge - frequency spectrum and for the occurence of unexpected areas of no discharge. This mechanism also leads to an understanding of why HVP can be used to detect materials of differing resistivity.

ACKNOWLEDGEMENTS

The author wishes to thank the North Carolina Academy of Sciences and the University of North Carolina at Wilmington for support given. He also would like to thank Dr. T. W. Haywood for his enthusiastic support of this work during the past two years. Without his aid and advice, this research would not have been possible to complete.

REFERENCES

* This work was supported by a Undergraduate Research Grant from the North Carolina Academy of Sciences and a Research Fellowship from the University of North Carolina at Wilmington.

(1) Tiller, W. A., Kirlian Photography: Its Scientific Foundations and Future Potentials, William A. Tiller, (1975), pp 3-9.

(2) Ibid.

(3) Moss, Thelma, The Probability of the Impossible: Scientific Discoveries and Explorations in the Psychic World, J. P. Tarcher, Inc, Los Angeles, CA, (1974).

(4) Tiller, pp. 3-9.

(5) Ibid.

(6) Boyers, D. G. and Tiller, W. A. "Corona Discharge Photography", Journal of Applied Physics, 44, 7, (1973), pp. 3102-3112.

(7) Ibid.

(8) Lord, David E., Electrical Discharge in Gases - A Technique for Detecting Metal Anomalies, University of California, Livermore CA, (1979), pp. 3-6.

(9) Lord, D.E. and Petrini, R.R., High-voltage Photography Applied to Non-destructive Testing., Lawerence Livermore Laboratory, Livermore, CA, Oct 8, (1975), p.2.

(10) Nielsen, N.J. and Shackelford, J.F., Non-destructive Inspection of Surface Topography by Electrical Discharge Imaging, to be published in International Advances in Non-Destructive Testing, Vol 8.

(11) Lord and Petrini, p.3.

(12) Ibid, p.5.

(13) Ibid, p.2.

(14) Nielsen and Shackelford, p. 12.

(15) Nielsen, J.N., Electrical Discharge Imaging, Thesis for Master of Science, University of California at Davis, Davis, CA, (1978), p.3.

(16) Boyers and Tiller, p. 3108.

SPONSOR OF THIS PAPER
Dr. T. W. Haywood
Physics Department
University of North Carolina at Wilmington
Wilmington, NC 28405

A SURVEY OF PROTO-PLANETARY NEBULAE AT THE OH MASER LINES

Bruce Brocka
St. Ambrose College
Davenport, IA 52803

ABSTRACT

Sixteen suggested proto-planetary nebulae were observed at all four OH maser lines (1612, 1665, 1667 and 1720 MHz) using the 18.3 m. radio-telescope at the North Liberty Radio Observatory. Some proto-planetary nebulae have also been classified as long period variables, as the optical and infra-red characteristics are similar. In some of these dually-classed objects, OH emission has been found. In planetary nebulae, however, no OH emission has been detected. In this survey, negative results were obtained, indicating that the presence or absence of OH may be used as a tool in classifying objects as proto-planetary nebulae.

INTRODUCTION

As the name suggests, proto-planetary nebulae are objects that are believed to be evolving into planetary nebulae. Proto-planetary nebulae have been characterized by Zukerman (1) as being very luminous red giants with large infra-red flux values and have a mass loss rate of about 10 solar masses per year. Their precursors possibly are Mira or semi-regular variable stars. A number of Mira variables are OH emitters, while OH surveys of planetary nebulae have had negative results (2,3,15). Similar observations of bipolar (symmetry about one axis) nebulae (4), possible progenitors of planetary nebulae (5) have had mixed results. A conclusion one can make is that the bipolar nebulae with OH emission do not evolve into planetary nebulae. This is to be expected as planetary nebulae are carbon-rich, and any oxygen present will likely form CO rather than OH. Radiation from CO is readily observable at millimeter wavelengths. It is used to classify objects as being carbon-rich. Many proposed proto-planetary nebulae are carbon-rich, but some are oxygen-rich. This implies that both have the characteristics necessary for 18 cm. OH emission.

As the presence or absence of OH emission seems to be a valid indicator of whether or not an object can be classified as a proto-planetary nebulae, 16 possible proto-planetary nebulae spectra were examined for OH emission. Normally in an OH survey, only the 1612 MHz line is examined. Numerous surveys (18) during the past decade have indicated that while terrestrially the 1665/7 MHz lines are the strongest, extra-terrestrially the strongest line is at 1612 MHz. In some cases, lines other than the 1612 line are not detectable. In a few rare cases, the 1720 line is the only one seen. For this survey, we decided to observe all four OH maser lines (1612, 1665, 1667, and 1720 MHz) to give a complete picture of the nebulae.

OBSERVATIONS AND RESULTS

The observations were carried out during August of 1979 with supplemental observations taken 10 December 1979 (M1-2 and CRL 618) and 21 May 1980 (CRL 618). The data were taken at the 18.3 m radio telescope at the North Liberty Radio Observatory which is owned and operated by the University of Iowa. The telescope was pointed in the proper direction and an intensity vs frequency spectrum was obtained. The receiver determined the frequency domain.

The flux calibration was done observing the OH lines of NML Cygni. This calibration insured that OH emission could be seen during the observing sessions.

It is also important that the antenna temperature be low. The antenna temperature creates a noise signal that sets the lower limit on the detectable flux. The root-mean-square (rms) value of the noise value determines the minimum detectable flux and hence gives a confidence interval. In keeping with the literature (16), the minimum detectable flux is taken to be three

times the rms noise (3σ). This means that there is a 99% confidence that any fluctuation greater than 3σ is a real signal. The rms noise is calculated using (16):

$$\sigma = \frac{\pi}{2} \cdot 21 \cdot \left[Ts / \sqrt{B \cdot t / A} \right] \text{ Jy } K^{-1}$$

where: B is the bandwidth, Ts is the system temperature, t is the integration time, and A is the number of autocorrelator channels. Typical integration times were between 45 and 60 minutes and generally a 1 MHz bandwith was used. The total unpolarized flux is related to the antenna temperature by a factor of 21 Jy K^{-1}. (1 Jansky (Jy) = 10^{-26} watts/m^2 and is a unit of intensity.) The system temperature was measured each observing session. This was accomplished using a calibration diode or observing the continuum spectrum of NML-Cyg.

FREQUENCY MHz	POLARIZATION	Ts K	LSR RANGE km/s	BANDWIDTH RESOLUTION km/s
1612	LHC	73	-93 to 93	2.91
1665/7	LHC	73	-90 to 90	2.81
1720	RHC	81	-86 to 86	2.72

TABLE 1
System Parameters for the lines used in the OH survey.

The measurements were frequency switched. For every minute the telescope was on the frequency of the source, it spent another minute examining a frequency that was off the source. This is a type of blank sky measurement. This measurement had a typical local standard of rest velocity of $\pm$ 90 km/s. The spectra were Hamming smoothed (17). A 128 channel autocorrelator was used. The specific system parameters for each line are given for each line in Table 1.

All observations were negative. No signal greater than 3σ was detected. The objects and their corresponding upper flux limits are listed in Table 2. Those fluxes marked with an asterisk indicate that it came from the literature, not from this experiment. Two anomalous observations of CRL 618 were made on 14 August 1979 and 10 December 1979. A peak of 5.3 to 6.6σ(about 3.5 Jy) at +21.1 km/s was observed. However, this structure was not confirmed by observations on 20 August 1979 and 21 May 1980. Figure 1 is the 14 August 1979 observation.

DISCUSSION

The absence of detectable OH emission from the proto-planetary nebulae would suggest that they are carbon rich. This supports the assertion that they are planetary nebulae progenitors. The list by Zukerman (1) is inhomogenous as three of the objects are oxygen rich : IRC+10011, NML Tau and IRC+60150; while the rest are carbon rich. The first two of these are known OH emitters and are commonly classed as long period variables. The last was examined as part of this survey. Its measured OH flux was not comparable with the first two mentioned above. Therefore, it still might be considered as a proto-planetary nebulae.

OBJECT	UPPER FLUX LIMIT (in Jy) 1612	1665	1667	1720	REFERENCE
R AND	1.6	1.5	1.5	1.8	1
MWC 17	1.5	1.8	1.8	1.8	7
MI-2	1.6	1.3	1.6	1.8	8
CRL 618	1.6	0.09*	0.09*	1.7	9
IRC+60150	1.6	1.6	1.6	2.0	1
MWC 574	1.2	1.5	1.5	1.8	10
AS 201	1.6	1.6	1.6	1.8	12
IRC+10216	0.15*	0.10*	0.10*	1.8	12
M2-9	0.2*	1.5	0.2*	1.8	13
IRC+20326	1.6	1.6	3.0	1.8	1
BF Cyg	1.6	1.6	1.6	1.8	1
HM Sge	1.6	0.03*	0.03*	2.0	9
X Cyg	1.6	1.6	1.6	1.8	1
V1016 Cyg	1.1	1.6	1.8	2.0	9
HBV 475	0.26*	0.09*	0.09*	2.9	9
CRl 2688	1.5	0.07*	0.07*	1.6	12

TABLE 2
Results of this experiment are presented here. Those values with asterisks are data taken from the literature to fill in the chart. It should be noted that these are essentially null results, indicating that there was no OH emission.

It appears that OH observations can be used as a diagnostic tool to determine if a nebula is not proto-planetary. The suggestion that Mira and other semi-regular variables are precursors of proto-planetary nebulae should perhaps be limited to those which do not have OH emission, e.g. symbiotic stars such as BF Cyg and V1016 Cyg.

REFERENCES

(1) Zuckerman, B., in Terzian,Y. (ed.) Planetary Nebulae, Observations and Theory, Reidel, Dorrecht, 1978.

(2) Turner, B.E., Ap. L, 8, (1971), p. 73.

(3) Zuckerman, B., et. al., Ap. J. 205, (1976), p. L15.

(4) Fix, J.D., and Mutle, R.L., Ap. L., 19 (1977), p. 37.

(5) Lo, K.Y., and Bechnis, K.P., Ap. J., 295 (1976), p. L21.

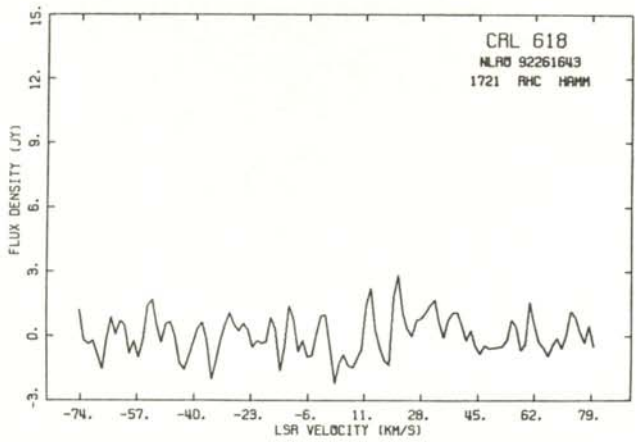

FIGURE 1
This is a typical output from the spectrometer showning the measured flux density in Janskys as a function of the local standard of rest velocity. This data was taken on 14 August 1979 from the source CRL 618. This output indicates that there is no measurable flux from the OH lines.

(6) Litvak, M.M., Ap. J., 156, (1973), p. 471.

(7) Allen, D.A., M.N.R.A.S., 161, (1973), p. 145.

(8) Cohen, M., and Barlow, M.S., Ap. J., 193, (1974), p. 401.

(9) Davis, L.E., Seaquist, E.R., Purton, C.R., Apl J., 230, (1979), p. 434.

(19) Sanduleak, N., and Stephenson, C.D., P.A.S.P., 84, (1972), p. 816.

(11) Sanduleak, N., and Stephenson, C.D., Ap. J., 220, (1978), p. 183.

(12) Fix, J.D., and Weisberg, J.M., Ap. J., 220, (1978), p. 836.

(13) Lepine, J.R., and Quang-Rieu, N., Astr. and Ap., 36, (1974), p. 139.

(14) Mammano, A., and Ciatti, F., Astr. and Ap., 39, (1975), p. 405.

(15) Terzian, Y., et. al., B.A.A.S., 10, (1978), p. 622.

(16) Kraus, J.D., Radio Astronomy, McGraw-Hill, New York, (1966).

(17) Blackman, R.B., and Tukeyk, J.W., Measurement of Power Spectra, Daver, New York, (1958).

(18) Cook, A.H., Clestial Masers, Cambridge, New York, (1977).

ACKNOWLEDGEMENTS

I would like to thank Dr. R.L. Mutel of the University of Iowa and Dr. T.B. Burns of St. Ambrose College for help in pursuing this work. I also acknowledge the work of fellow students B.K. Edgar and S. Carroll for taking the supplemental observations.

SPONSOR FOR THIS PAPER

Dr. Thomas Burns
Physics Department
St. Ambrose College
Davenport, IA 52803